Green Chemistry

PAPER

View Article Online
View Journal | View Issue

Cite this: *Green Chem.*, 2022, **24**, 9114

Hydrogels with protective effects against cellular oxidative stress *via* enzymatic crosslinking of feruloylated arabinoxylan from corn fibre†

Secil Yilmaz-Turan,[a] Kun Jiang,[a,b,c] Patricia Lopez-Sanchez,[d,f] Amparo Jiménez-Quero,[a] Thomas Crouzier,[a,b,c] Tomás S. Plivelic[e] and Francisco Vilaplana *[a]

Biocatalytical upgrading of side streams from agricultural biomass into multifunctional materials constitutes a very attractive option to increase the circularity of food and material systems. We propose the design of radical scavenging hydrogels with mechanical integrity and protective effects against reactive oxygen species by enzymatic crosslinking of arabinoxylans (AX) with high ferulic acid content extracted from corn fibre using subcritical water. We have compared the influence of two enzymatic systems, laccase/O_2 and peroxidase/H_2O_2, on the biochemical structure, multiscale assembly, physicochemical properties, and radical scavenging activity of the polysaccharide hydrogels. Peroxidase crosslinking results in instant hydrogel formation, whereas laccase shows slower crosslinking kinetics, resulting in a more elastic gel network. Characterization by size exclusion chromatography, small angle X-ray scattering, and microscopy revealed structural differences in the network organization of the hydrogels produced by the two enzymes. Laccase crosslinking leads to smaller polymeric aggregates, promoting their progressive organization in network clusters that impact the overall ultrastructure. Conversely, the fast crosslinking induced by peroxidase results in higher porosity and forms larger and potentially more heterogeneous aggregates, which seem to hinder their subsequent association in clusters. Both AX hydrogels exhibit adequate biocompatibility and protective effects against *in vitro* cellular oxidative stress compared to an alginate reference. This constitutes a proof of concept of the potential application of radical scavenging hydrogels from agricultural side streams for biomedical and nutritional applications in wound healing, cellular repair and targeted delivery.

Received 4th September 2022,
Accepted 3rd November 2022

DOI: 10.1039/d2gc03331c

rsc.li/greenchem

Introduction

Globally, approximately 38% of food produced is lost and wasted throughout the entire food value chain, which accounts for 8 to 10% of the total greenhouse gas emissions.[1,2] However, agricultural losses and food waste constitute a rich but complex and heterogenous source of biomolecules (metabolites and macromolecules); this presents a valuable opportunity for their biotechnological upgrading into functional materials for a wide range of advanced applications.[3] In this context, corn is the largest staple cereal worldwide, with an annual production of 1200 million tonnes.[4] Corn wet milling generates large volumes of side streams such as corn fibre (also referred to as corn bran), which contains large volumes of cell wall polysaccharides such as arabinoxylans (AX) accounting for 30–50% (of dry weight) depending on the source.[5] Corn bran AX holds therefore great potential as versatile polymeric matrix for the development of functional materials, due to its availability and its complex molecular

[a]*Division of Glycoscience, Department of Chemistry, School of Engineering Sciences in Chemistry, Biotechnology and Health, KTH Royal Institute of Technology, AlbaNova University Centre, SE-106 91 Stockholm, Sweden. E-mail: franvila@kth.se*
[b]*AIMES – Center for the Advancement of Integrated Medical and Engineering Sciences at Karolinska Institutet and KTH Royal Institute of Technology, Stockholm, Sweden*
[c]*Department of Neuroscience, Karolinska Institutet, SE-171 77 Stockholm, Sweden*
[d]*Division of Food and Nutrition Science, Biology and Biological Engineering, Chalmers University of Technology, SE-412 96 Gothenburg, Sweden*
[e]*MAX IV Laboratory, Lund University, PO box 118, 221 00 Lund, Sweden*
[f]*Food technology, Department of Analytical Chemistry, Nutrition and Food science. University of Santiago de Compostela, Campus Terra, 27001 Lugo, Spain*

†Electronic supplementary information (ESI) available: Composition of arabinoxylan extracted from corn bran (Table S1), phenolic acid profiles of native and crosslinked arabinoxylan (Fig. S1), ion extracted HPLC-ESI-MS chromatograms of the standard mixture and CID-MS^2 spectra of ferulic acid dehydrodimers (Fig. S2), CID-MS^2 spectra of ferulic acid dehydrodimers detected in native and crosslinked arabinoxylan (Fig. S3), ion extracted HPLC-ESI-MS chromatograms of ferulic acid dehydrotrimers (Fig. S4), molar mass distributions of native and crosslinked arabinoxylan at higher concentrations (Fig. S5); wide-angle X-ray scattering (WAXS) profiles of CAX solutions and hydrogels (Fig. S6). See DOI: https://doi.org/10.1039/d2gc03331c

structure in terms of the high degree of substitution of the polymeric backbone, the presence of oligomeric decorations, and the high abundance of hydroxycinnamic acids covalently bound to the polysaccharide core (Fig. 1a).

Hydrogels are three-dimensional polymeric matrices that can retain large amounts of water in their network. Polysaccharides show great potential as matrices for hydrogel production, due to their hydrophilic, biodegradable and biocompatible nature, which make them suitable for food and biomedical applications. Polysaccharide hydrogels can be formed through physical approaches (*e.g.* temperature, salt- or pH-gelation)[6] or by chemical/enzymatic crosslinking.[7] Hydrogels developed from plant polysaccharides (*e.g.* xylan, xyloglucan and glucomannan) are non-cytotoxic and they can be used for drug release and encapsulation of fibroblasts, demonstrating their ability to establish or support load-bearing biological scaffolds.[8–10] Upon use in biomedical applications, it is desirable that polysaccharide hydrogels combine mechanical integrity with bioactive properties. In this direction, the use of hydrogels as radical scavenging biomaterials against reactive oxygen species (ROS) constitutes a promising route to mitigate oxidative stress and derived inflammation responses in different pathogenic processes. Radical scavenging hydrogels usually consist of polymeric matrices that embed in their structure either scavenging inorganic particles[11] or organic compounds such as free phenolic moieties.[12,13]

Ferulic acid (FA) is the predominant phenolic group in corn bran AX and can reach up to 4% of dry weight.[14] In cereal cell walls, FA units covalently crosslink adjacent AX chains through dimerization reactions, forming dehydrodimers (di-FAs) and dehydrotrimers (tri-FAs).[15] As we have previously demonstrated, feruloylated AX can be extracted with high yields from corn bran using subcritical water extraction (SWE), maintaining their polymeric structure and tuning the degree of substitution depending on the extraction conditions.[16] Additionally, SWE preserves the FA moieties covalently bound to the AX, conferring inherent bioactive properties (*e.g.* antioxidant activity) to these polysaccharides[16–18] that could be exploited to design radical scavenging biomaterials. Such FA moieties can be used for the development of stable polysaccharide hydrogels mimicking plant cell wall formation, *via* dimerization reactions using oxidative enzymes such as laccase and peroxidase (Fig. 1b).[19,20] The crosslinking mechanisms by the two enzymes are different, since the copper cluster of laccase directly interacts with oxygen, whereas peroxidase requires hydrogen peroxide to oxidize the substrate.[21] The distinct oxidation mechanisms of the two enzymes depend on the structural features of the substrate polysaccharides, such as FA content and branching structure, which in the end influence the kinetics of the crosslinking reaction and the structural and functional properties of the resulting hydrogels.[22–24] Therefore, fundamental understanding of the gelation mechanisms upon enzymatic crosslinking and their multiscale assembly of the hydrogels will contribute to tailor their performance, particularly for biomedical applications that need specific properties in terms of mechanical performance and bioactivity.

The aim of the study is to prepare radical scavenging hydrogels by enzymatic oxidative coupling of AX from corn bran, exploiting the presence of phenolic moieties covalently bound to the polysaccharide core. This approach presents large benefits compared to other phenolic-containing biomaterials, as they can be prepared in a one pot biocatalytic process without the use of external additives or catalysts. The biochemical performance of laccase and peroxidase has been monitored in terms of the changes in the monomeric and dimeric FA profiles over time. We also studied the mechanisms for *in situ* hydrogel formation in terms of rheological performance and multiscale assembly from the molecular to the microstructural level. Finally, as a proof of concept, we aim to demonstrate *in vitro* the protective effects of the AX hydrogels against oxidative stress on human colon cells. This paves the way for the potential biomedical application of the enzymatically crosslinked hydrogels as biomaterials in the prevention of early stages of inflammation caused by reactive oxygen species.

Material and methods

Materials

Corn bran was provided by Cargill Deutschland GmbH (Krefeld, Germany). The 5–5′ and 8–8′ dehydrodimers of FA were kindly gifted by Prof. Florent Allais and Amandine Léa Flourat (AgroParisTech, Pomacle, France). All chemicals, reagents and enzymes were purchased from Sigma Aldrich (Stockholm, Sweden).

Extraction of arabinoxylan from corn bran

Destarching of corn bran and subcritical water extraction (SWE) was performed on the pilot plant by Celabor (Chaineux, Belgium), using process conditions previously developed in our laboratory.[25] Destarching was carried out by mixing the corn bran with hot water for 4 h at 80 °C, followed by filtration through a 25 μm sieve and manual pressing of the solid residue resulting in a wet destarched corn bran cake. The destarched corn bran cake was then loaded in the reactor and mixed with tap water at a ratio of approximately 1 : 15. SWE was performed for four sequential cycles of 10, 30, 60 and 90 min at 160 °C. During all the extraction cycles, water was circulated through the biomass using a pump to ensure complete mixing. The extracts obtained after each extraction cycle were pulled together and then freeze-dried. The resulting corn bran extract was named as CAX. The monosaccharide composition, soluble protein, and phenolic acid content of CAX is presented in ESI Table S1.†

Enzymatic crosslinking of arabinoxylan

The crosslinking of CAX was carried out using laccase from *Trametes versicolor* (EC 1.10.3.2) and peroxidase from horseradish (*Amoracia rusticana*) (HRP) (EC 1.11.1.7). CAX was

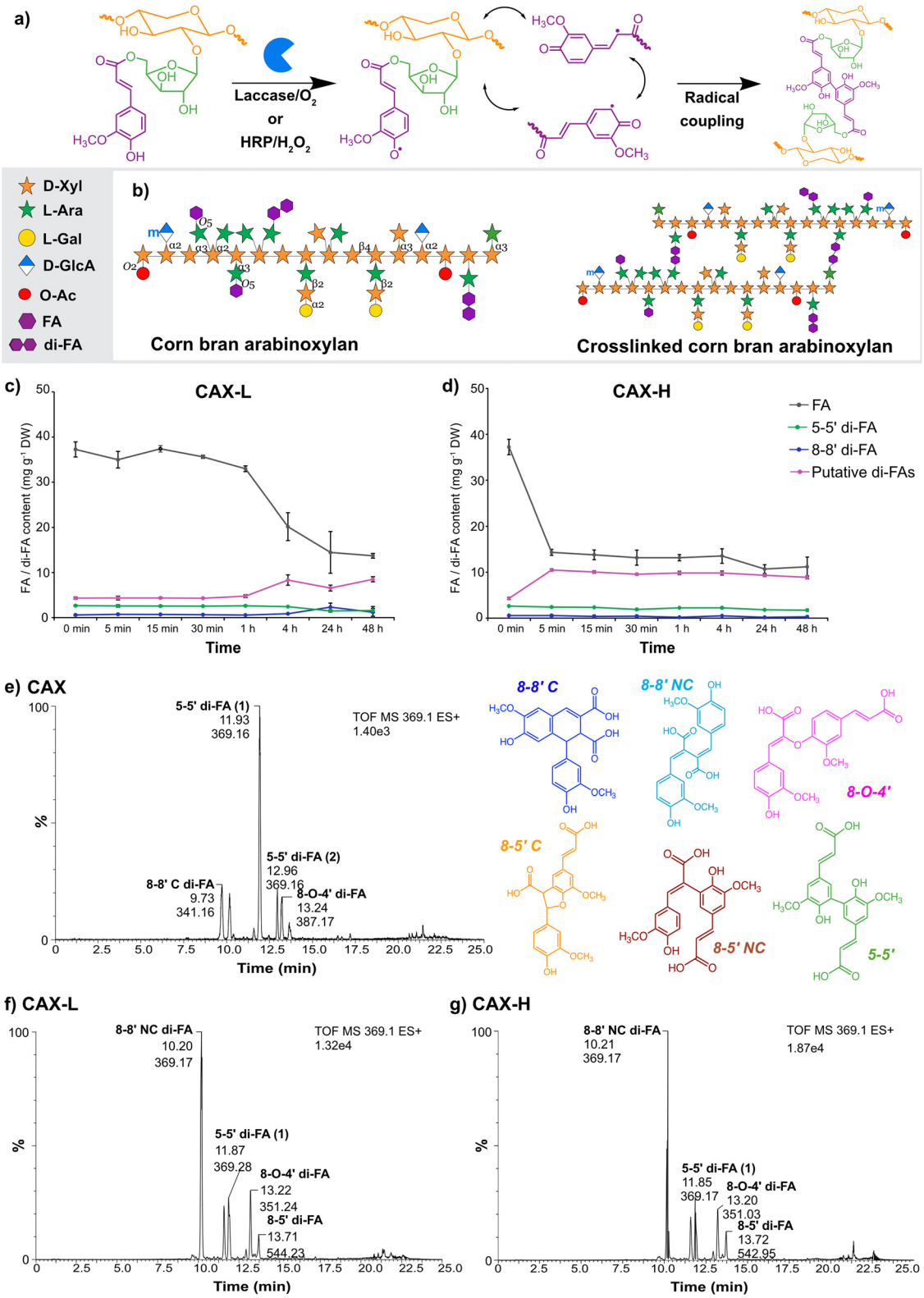

Fig. 1 (a) Mechanism for the crosslinking reaction of ferulic acid (FA) by laccase and HRP, originating feruloyl dimers (di-FAs). (b) Molecular structure of feruloylated AX from corn bran. Corn bran AX is composed of a (1 → 4)-linked-β-D-xylopyranosyl (Xyl) backbone, with substitutions of α-L-arabinofuranose (Ara) at the C(O)-3 and/or the C(O)-2 positions, and α-D-glucuronic acid (GlcA) or its derivative 4-*O*-methyl-D-glucuronic acid (*m*-GlcA) at the C(O)-2 position. The complexity of corn bran AX arises from further oligomeric substitutions to the Ara side chains, composed of Xyl or galactose (Gal) moieties. Corn bran AX is additionally esterified to acetyl and phenolic groups. Time evolution of the depletion of FA and formation of di-FAs during enzymatic crosslinking by (c) laccase (CAX-L) and (d) HRP (CAX-H). Ion extracted HPLC-ESI-MS chromatogram of (e) CAX, (f) CAX-L and (g) CAX-H. The mass to charge ratio of the di-FA peaks were assigned to [M − H_2O + H^+].

dispersed in ultra-pure water at room temperature at 5% (w/v) for both laccase and HRP crosslinking. CAX solution was mixed with laccase solution (1.675 nkat mg^{-1} AX) for laccase crosslinking, and with HRP solution (0.510 nkat mg^{-1} AX) and 30% H_2O_2 (33 μL mL^{-1} CAX solution) for HRP crosslinking, respectively. The polysaccharide concentration (5% w/v) and enzyme dosing were selected based on preliminary optimization of the system (results not shown).[26] The hydrogels were formed at 30 °C under constant stirring (200 rpm). The laccase- and HRP-crosslinked samples were named as CAX-L and CAX-H respectively.

Biochemical characterization of the enzymatic crosslinking

Quantification of phenolic acids by HPLC-UV. The ester-linked phenolic acid content of the samples was determined by HPLC after saponification. CAX-L and CAX-H were freeze-dried after crosslinking for 4 h and dry CAX, CAX-L and CAX-H were saponified in dark microcentrifuge tubes (Eppendorf, Hamburg, Germany) using 2 M NaOH (20 : 1, w/v) at 30 °C overnight and then acidified by 37% HCl. The samples were then extracted by ethyl acetate (2 : 1 v/v) and the pulled extracts were dried under nitrogen. Dried samples were resuspended in methanol: 2% acetic acid mixture (1 : 1 v/v) and injected onto the HPLC system (Waters 2695 separation module, Waters 2996 photodiode array detector; USA) coupled to a UV/Vis detector, equipped with a C18 guard column and an SB-C18 separation column (Zorbax SB-C18 5 μm particle size, 4.6 × 250 mm, Agilent, USA) at 1 mL min^{-1} using a gradient of 2% acetic acid and methanol.[27] Caffeic acid, *p*-coumaric acid, ferulic acid, cinnamic acid, 5–5′ di-FA and 8–8′ di-FA at concentrations between 0.005 g L^{-1} and 0.1 g L^{-1} were used for the standard calibration recorded at 270 nm and 325 nm.

The time evolution of the crosslinking by laccase and HRP was also monitored using HPLC analysis. CAX was mixed with respective enzymes and the reaction was stopped at 5, 15 and 30 min and 1, 4, 24 and 48 h. The crosslinked samples were then saponified and the FA and di-FA content was quantified using the same HPLC system as described above in triplicate.

Profiling of di-FA by tandem LC-ESI-MS/MS. The identification of FA dehydrodimers (di-FAs) was performed after saponification as described above. Saponified CAX, CAX-L and CAX-H were suspended in 50% acetonitrile supplemented with formic acid (0.1% v/v) and injected onto an HPLC system equipped with an Eclipse Plus C18 column (Agilent Technologies, Santa Clara, CA, USA) and coupled to an electrospray ionization mass spectrometry (ESI-MS) using a Synapt G2 mass spectrometer (Waters, Milford, MA, USA) in positive mode. Capillary and cone voltage were kept at 3 kV and 10 kV, respectively. 0.1% (v/v) formic acid in water (Eluent A) and 0.1% (v/v) formic acid in acetonitrile (Eluent B) were used as the mobile phase. The eluent program was as follows: 95% A (2 min), 62% A (15 min), 10% A (3 min), 10% A (1 min), 95% A (5 min) and 95% A (1 min). A standard mixture of monomeric FA, 5–5′ di-FA and 8–8′ di-FA was used at 0.1 mg mL^{-1} to determine the reference retention times of the di-FAs in the samples. MS^2 analysis was performed in positive mode with ion collision induced dissociation (CID) using argon as the collision gas. The fragmentation of the di-FAs was done using 369.1 *m*/*z* ion subjected to a collision energy of 20 eV. The MassLynx software (Waters, Milford, MA, USA) was used for the processing of the chromatograms and spectra.

Molar mass distributions by SEC-MALLS. The molar mass distributions of CAX, CAX-L and CAX-H were determined by size exclusion chromatography (SECcurity 1260, Polymer Standard Services, Mainz, Germany) coupled to a multi-angle laser light scattering (MALLS) detector (BIC-MwA7000, Brookhaven Instrument Corp., US) and a refractive index detector (SECcurity 1260, Polymer Standard Services, Mainz, Germany) termostatted at 45 °C. Freeze-dried samples were dissolved in the SEC eluent (DMSO supplemented with 0.5% (w/v) LiBr) at concentrations of 0.5, 1.0 and 2.0 mg mL^{-1}, filtered through nylon syringe filters (0.2 μm) and then injected onto the SEC at a flow rate of 0.5 mL min^{-1} with GRAM 30 and 10 000 analytical columns (PSS, Mainz, Germany). Pullulan standards (342–708 000 Da) (PSS, Mainz, Germany) were used for the standard calibration of the size distributions. The elution volumes from the SEC separation were converted into hydrodynamic volumes (V_h) using the Mark–Houwink equation.[28] The Mark–Houwink parameters for pullulan in DMSO-LiBr are $K = 2.427 \times 10^{-4}$ dL g^{-1} and $a = 0.6804$ (Kramer and Kilz, PSS, Mainz, Germany, private communication). The data is presented in terms of hydrodynamic radius (R_h), corresponding to the equivalent of hydrodynamic volume with $V_h = 4/3\pi {R_h}^3$.[28]

Functional and structural characterization of hydrogels

Rheology. The time evolution of the gelation by laccase and HRP was monitored using a strain-controlled rheometer (Discovery HR3, TA Instruments, New Castle, DE, USA) at 25 °C with a 25.0 mm parallel plate and 1 mm gap. The respective enzyme was added to the CAX solution (5% w/v) and mixed; H_2O_2 addition followed in the case of HRP-crosslinking. The mixture was then immediately placed onto the rheometer. The edges of the samples exposed to the air were covered with parafilm oil to prevent drying during measurements. The storage (G') and loss (G'') modulus values were monitored for 2–5 h at a frequency of 6.3 rad s^{-1} and 1% oscillation strain. The viscoelasticity measurements (in duplicates) were carried out at the end of the gel formation using a frequency sweep from 0.1 to 100 rad s^{-1} and 1% oscillation strain.

Cryogenic scanning electron microscopy (Cryo-SEM). The morphology of the hydrogels was characterized by cryogenic scanning electron microscopy (cryo-SEM). The hydrogel samples prepared by high pressure freezing (HPF) using an HPM100 system (Leica Microsystems, Wetzlar, Germany). A piece of sample hydrogel was carefully loaded onto 6 mm aluminum sample platelets and then frozen at high pressure (HPF). Afterwards, frozen samples were transferred to liquid nitrogen and stored until analysis. Prior to cryo-SEM imaging, the frozen samples were sublimated *in vacuo* at −90 °C for

30 min and then coated with Pt for 10 s. The imaging was conducted using a field emission scanning electron microscopy (FE-SEM) (Merlin, Carl Zeiss GmbH, Germany) fitted with a PP3000T cryo-SEM preparation system (Quorum Technologies, UK) at −140 °C using in-chamber secondary electron detector (ETD) at acceleration voltage of 3 kV and probe current of 50 pA. The porosity values of the hydrogels were calculated by the ratio of the total pore area of each image to the total image area, and the area of each pore was automatically measured using the open-source CellProfiler™ software (4.2.0).

Wide-angle (WAXS) and small angle X-ray scattering (SAXS). WAXS/SAXS measurements were carried out using a laboratory-based X-ray source Rigaku 003+ high brilliance microfocus with Cu-radiation source, λ = 1.54 Å (Rigaku Corp., Tokyo, Japan). CAX solution was measured in sealed quartz capillaries (2 mm diameter, 0.01 mm wall thickness) (Hilgenberg Gmbh, Germany) and the hydrogels (CAX-L and CAX-H) were analyzed in sandwich cell holders constrained by a Kalrez O-ring (5.28 mm inner diameter, 1.78 mm thickness) and 15 μm Mica/Kapton windows. The WAXS and SAXS scattering was recorded under vacuum with an approximate sample-detector distance of 132 mm and 1084 mm, respectively, given the scattering vector q-range between $0.007 < q < 0.27$ Å^{-1} (where $q = (4\pi/\lambda)\sin(\theta)$ and 2θ is the scattering angle). The calibration of the systems was performed using the scattering from the reference sample silver behenate. The scattering from an empty quartz capillary, quartz capillary filled water, an empty sandwich cell holder and sandwich cell holder with mica were recorded as the respective background. The 2D SAXS pictures were recorded using a Pilatus 300K detector (Dectris, USA). The background was subtracted using the ATSAS software package[29] and the data was analyzed using the SasView software.[30]

***In vitro* assessment of cell response to the exposure to CAX hydrogels under oxidative stress.** HT29-MTX (CelluloNet Biobank BB-0033-00072 facility of SFR Biosciences, France) cells were employed as the model cell line to evaluate the cytocompatibility of the CAX hydrogels and the response under oxidative stress. We selected the HT29-MTX cell model due to its relevance for human gastrointestinal studies and their improved mucus layer formation, which results in better mimicking of physiological conditions in the gut.[31] Alginate gel was used as negative control, which was formed by adding 10 μL of 10% (w/v) $CaCl_2$ to 100 μL of 2% (w/v) sodium alginate, giving a final $CaCl_2$ concentration of 1%. Alginate gel was then washed sufficiently with phosphate buffered saline (PBS) to remove excess $CaCl_2$ and sterilized by UV. HT29-MTX cells were cultured in T-75 tissue culture flasks (Sarstedt) with Gibco Dulbecco's Modified Eagle's (DMEM-F12) medium (phenol red, with GlutaMax, ThermoFisher) supplied with 10% (v/v) heat-inactivated fetal bovine serum (FBS) and penicillin/streptomycin (P/S, 100 U mL^{-1}, ThermoFisher) in a humidified incubator with 5% CO_2 at 37 °C. For sterilization, the CAX powder was exposed to UV for 2 h, sodium alginate solution was sterilized in an oven at 120 °C for 1 h and $CaCl_2$, laccase and HRP solutions were filtered through 0.2 μm syringe filters before crosslinking. CAX-L, CAX-H and alginate gels were formed (50 μL) in 96-well plates by adding corresponding enzymes and solutions. The plates containing the gels were further sterilized by UV in a laminar hood for 30 min and then washed with the DMEM/F-12 without phenol red with 10% FBS and 100 u mL^{-1} P/S (the medium without phenol red) overnight at 4 °C. The washing medium was removed before seeding the cells.

The production of cellular reactive oxygen species (ROS) was measured using the 2′,7′-dichlorofluorescin diacetate (DCFDA/H2DCFDA) Cellular ROS Assay Kit (Abcam 113851, Amsterdam, Netherlands). The gels were incubated with 50 μL *tert*-butyl hydroperoxide (TBHP) in the medium without phenol red at concentrations of 0, 0.15, 0.6, 3, 6, 15 and 30 mM at 37 °C for 1 h to allow the diffusion of TBHP into the gels. The excess solution was removed before seeding the cells at 10^4 cells/well. Separately, the cells were detached from the flask with accutase (400–600 units per mL, Sigma A6964), washed with the ROS assay working buffer, and incubated in 10 μM of DCFDA reagent at 37 °C for 30 min in the dark. The cells were then washed with PBS and diluted to 1×10^5 cells per mL in the medium without phenol red. A volume of 100 μL of the cells was added onto each gel and the plates were kept at 37 °C for 20 min for the cells to settle down. The fluorescence was then measured every 30 min for 3 h at 492/517 nm. Gels treated with TBHP and incubated only with the cell medium were used as blank.

The viability of the cells after oxidative stress by TBHP was determined using the Alamar Blue cell viability assay (Invitrogen, ThermoFisher Scientific, Sweden). The cells were seeded (1×10^4 cells per gel) on the gels equilibrated with TBHP at corresponding concentrations, and further incubated for 3 h. A volume of 10 μL of Alamar Blue reagent was then added to each well, the plates were incubated at 37 °C for 2 h, and the fluorescence was recorded at 560/590 nm using a microplate reader (Clariostar Plus, BMG LABTECH, Ortenberg, Germany). The TBHP-loaded gels incubated only with the cell medium were used as blank.

Results and discussion

Laccase and horseradish peroxidase generate similar dimeric profiles with different timeframes

The enzymatic crosslinking of feruloylated arabinoxylan has mainly focused on the use of laccases.[32,33] However, the choice of the crosslinking system (*i.e.* laccase/O_2 or peroxidase/H_2O_2)[23] and the source of the enzyme[20] influence the properties of the resulting hydrogels. In this study, we compared biochemically the distinct crosslinking mechanisms by laccase and peroxidase, by monitoring the content of monomeric FA and its dehydrodimers (di-FAs) during the enzymatic process. In agreement with previous studies,[16,34] the phenolic acid content of the starting CAX substrate was particularly rich in FA, with lower content of *p*-coumaric acid, sinapic acid and di-FAs such as 5–5′ and 8–8′ (Table 1). Other peaks were observed

Table 1 Phenolic acid content of native and crosslinked corn bran arabinoxylan

Phenolics (mg g^{-1} DW)	CAX	CAX-L[a]	CAX-H[a]
p-Coumaric acid	2.0 ± 0.1	1.8 ± 0.1	1.8 ± 0.0
Sinapic acid	1.2 ± 0.0	0.9 ± 0.2	1.2 ± 0.1
Ferulic acid	36.1 ± 1.6	13.7 ± 0.5	11.9 ± 2.1
8–8′ di-FA	0.7 ± 0.2	0.5 ± 0.2	0.3 ± 0.2
5–5′ di-FA	2.6 ± 0.1	1.6 ± 0.9	1.7 ± 0.2
Putative di-FAs[b]	4.4 ± 0.3	8.5 ± 0.2	8.9 ± 0.3
Total	47.1 ± 0.3	29.4 ± 5.1	30.8 ± 0.2

[a] Phenolic acid content of CAX-L and CAX-H was measured after 48 h of the crosslinking to ensure the steady state in the crosslinking of AX by both enzymes. [b] The unknown di-FAs in HPLC chromatograms were combined as putative di-FAs and their amount was estimated using the response factor of 8–8′ and 5–5′ di-FAs.

in the HPLC chromatogram eluting after the 8–8′ di-FA (29.3 min) and 5–5′ di-FA (40.0, 40.7 and 40.9 min), which were not quantified due to the lack of standards (Fig. S1a†). These unassigned peaks were attributed to other forms of di-FAs, namely the 8-*O*-4′ and 8–5′ di-FAs, as these di-FAs have been reported to be present in corn bran AX.[20] To estimate the amount of these unknown di-FAs, we used the response factors of the 8–8′ and 5–5′ di-FAs and combined those as putative di-FAs (Table 1). CAX therefore contains considerable amounts of putative di-FAs, accounting for 4.4 mg g^{-1} AX, which are expected to be involved in the enzymatic crosslinking reaction.

Laccase and HRP crosslinking caused a significant decrease of the monomeric FA content (Fig. S1b and S1c†), oxidizing 62% and 67% of the initial FA monomers, respectively, followed by an enrichment of the total di-FA content in CAX-L and CAX-H (Table 1). Comparing the relative contents of the different ferulic acid dimers upon crosslinking, the amount of the 5–5′ di-FA decreased, the 8–8′ di-FA content was kept constant, and the amounts of putative di-FAs increased by 2-fold. As the total amount of formed di-FAs was not proportional to the depletion of the monomeric FA in both CAX-L and CAX-H, the formation of dehydrotrimers of FA (tri-FAs) from the existing di-FAs (5–5′ and 8–8′) may have occurred.[19] Moreover, the higher conversion ratio of monomeric FA achieved by HRP together with the similar di-FA content to laccase, implied that the HRP-crosslinking possibly formed higher number of tri-FAs (as discussed later). These results demonstrate that different oxidative enzymes are capable of oxidizing different positions of the FA molecule, resulting in the conversion of monomeric FA into various di-FAs and presumably tri-FAs. The oxidation and radical coupling, however, appears to proceed randomly as a different abundance of di-FAs has been previously reported in corn bran AX crosslinked by the same enzymes used in our study.[23]

The time evolution of the enzymatic crosslinking of CAX-L showed that the FA content gradually decreased and became constant approximately at 24 h (Fig. 1c). This was also the time point when the di-FA content reached a plateau. Interestingly, the lower FA content of CAX-H was attained almost instantly at 5 min (Fig. 1d). It should be noted that the dosage of HRP (0.510 nkat mg^{-1} AX) used for the crosslinking was lower than that of laccase (1.675 nkat mg^{-1} AX), suggesting that HRP is a more effective oxidative catalyst than laccase even at lower concentration. The results of the time evolution of crosslinking indicated that the oxidative coupling of FA by H_2O_2 catalyzed by HRP is much faster than the reaction occurring *via* electron transfer in a copper cluster in laccase, in agreement with previous studies.[23,24,35]

In order to identify the unknown di-FAs observed in the HPLC chromatograms (putative di-FAs) and potential tri-FAs, HPLC-ESI-MS^2 of CAX, CAX-L and CAX-H were analyzed (Fig. 1e–g). In the HPLC-ESI-MS^2 profile of CAX (Fig. 1e) six different forms of di-FAs were observed, and the CID-MS^2 fragmentation of the peaks was assigned to the individual di-FA peaks namely the 8–8′ cyclic (C), 8–8′ non-cyclic (NC), two forms of 5–5′, 8-*O*-4′ and 8–5′ NC di-FAs according to Vismeh, *et al.*[36] (ESI, Fig. S3†). This confirmed that four different forms of di-FAs aside from the 8–8′ and 5–5′ di-FAs were indeed present in CAX. Amongst the different di-FAs, the 5–5′ di-FA had the highest peak intensity, which was in alignment with the HPLC results. Regarding the laccase-crosslinking, differences were observed in the HPLC-ESI-MS^2 spectra of CAX-L both in the presence and the intensity of the peaks (Fig. 1f) compared to that of CAX. The peak eluting at 9.7 min in CAX was not present in CAX-L, and the intensity of the peaks at 11.9 and 12.9 min significantly decreased in CAX-L. This indicated that the 8–8′ C and 5–5′ di-FAs converted to other FA bridges with crosslinking. On the other hand, the peak intensities of two different forms of the 8–8′ NC di-FA (10.2 and 11.6 min) and the 8-*O*-4′ di-FA (13.2 min) increased in CAX-L. Additional small peaks were observed in CAX-L at 13.5 and 13.6 min, corresponding to the 8–5′ C di-FA; however, these were minor and the 8–5′ NC di-FA was the dominant form. As for the HRP-crosslinking (Fig. 1g), identical changes as in CAX-L were seen in the presence and the intensity of the di-FA peaks in CAX-H. These results did not explain the higher conversion ratio of FA monomers by HRP crosslinking (67%) than that of laccase (62%). Therefore, the presence of tri-FAs was also monitored. The molecular mass of tri-FAs was determined as 579 g mol^{-1} according to Bunzel, *et al.*[37] and the peaks were identified by the 579 *m*/*z* ion (ESI, Fig. S4†). Compared to CAX, increased intensities of the tri-FA peaks (10.58, 11.34, 11.68, 12.73, 13.72 and 15.01 min) were observed in CAX-L and CAX-H, verifying the formation of tri-FAs when crosslinking was applied. Furthermore, the presence of higher amounts of tri-FAs in CAX-H was detected as the peak intensities were higher for CAX-H than that for CAX-L, especially at 11.34 and 15.01 min. This may explain the higher conversion ratio of monomeric FA by HRP due to the formation of higher numbers of tri-FAs as observed by HPLC. This demonstrated the successful oxidation of FA monomer by laccase and peroxidase, which resulted in similar di-FA and tri-FA profiles as shown by HPLC-ESI-MS^2 analysis.

Peroxidase and laccase distinctly influence the gelation kinetics and the rheological properties

The development of storage (G') and loss (G'') moduli of the hydrogels over time was studied by small amplitude oscillatory shear (Fig. 2a). The viscoelasticity of the CAX-L and CAX-H hydrogels at the end of the gelation reactions is shown in Fig. 2b. When crosslinked by laccase (CAX-L), a lag phase of G' was observed for approximately 65 min, after which a first slight increase (between 65–90 min) was seen and then a sharp increase followed (90 min). Eventually, a slowing down tending to a plateau (G' = 112 Pa) was reached at approximately 200 min. The time point at G' started to increase corresponded to the time point that the monomeric FA content started to decrease and di-FA content started to increase (Fig. 1c). On the other hand, G' of CAX-H increased instantly following the addition of H_2O_2 to the system, making it impossible to measure the time development of the dynamic moduli of this hydrogel (that is, CAX-H was already a gel when the measurement was started). This, in fact, agreed with the rapid depletion of the FA monomers and increase in the di-FA content reported by the biochemical analyses (Fig. 1d). The time evolution of the gelation of both CAX-L and CAX-H indicated that the development of the mechanical strength of the hydrogels is directly related to the increased density of the covalent bonds formed between FA units of the adjacent AX chains.

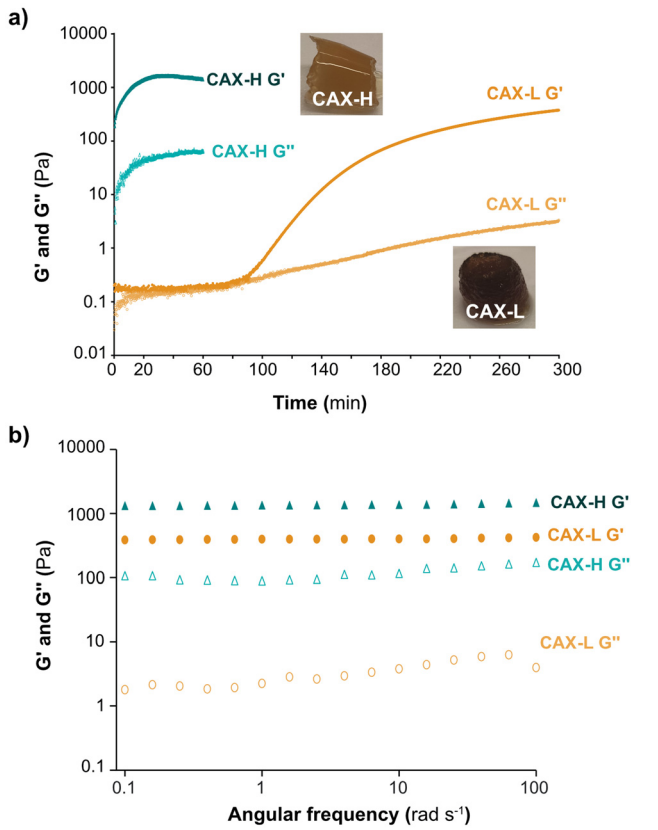

Fig. 2 Rheology of native and crosslinked corn bran arabinoxylan. (a) Time evolution of G' and G'' during gelation by laccase (CAX-L) and HRP (CAX-H); (b) storage (G') and loss moduli (G'') of CAX, CAX-L and CAX-H.

The mechanical spectra of CAX-L and CAX-H after the gelation reactions revealed a gel-like behavior with $G' > G''$ (Fig. 2b) and G' values independent of the measured frequency (0.1–100 rad s^{-1}). The G'' values were slightly dependent on frequency, which can be attributed to physical interactions in the hydrogel networks.[38] Comparing the mechanical spectra of the two hydrogels, CAX-H had a higher G' than that of CAX-L (3.5 fold) and its G'' was significantly higher (100 fold). Importantly, the comparison of loss tangent ($\tan\delta$) of the two hydrogels revealed differences in terms of their network structure. Tan δ is described as the ratio between G'' and G' and provides information about the network strength of materials. When $\tan\delta < 1$, elastic properties prevail, indicating gel or solid-like network; when $\tan\delta > 1$, viscous contribution is dominant, implying fluid or liquid-like state. The $\tan\delta$ of CAX-L was 10-fold lower than that of CAX-H, which revealed that CAX-L had a more elastic network. This was interesting as both CAX-L and CAX-H contained a similar number of covalent crosslinks as revealed by the quantification of FA and di-FAs (Table 1). We hypothesize that the distinct rheological behavior of the two hydrogels can be attributed to chemical and physical factors. First, laccase and peroxidase induce distinct relative placement of the new crosslinks between CAX polymers, where HRP may induce the covalent crosslinking of a larger number of polymeric chains compared to laccase, as we hypothesize from the results of the hydrodynamic conformations and molar mass by SEC-MALLS. This, in turn, creates a less organized network for CAX-H compared to CAX-L, which may result in lower elasticity of the CAX-H hydrogel. Secondly, the slower action of laccase progressively promotes non-covalent interactions between polymers that can act as nucleating agents for their further supramolecular assembly in stable aggregates, which contribute to the formation of a more elastic network in CAX-L. These hypotheses are further discussed in the context of the multiscale characterization of the network structure of the hydrogels.

Laccase and peroxidase crosslinking result in distinct multiscale network architectures

The structural and morphological properties of the CAX solution and the laccase- (CAX-L) and HRP-crosslinked (CAX-H) hydrogels were characterized at the different length scales, from the macromolecular to the network levels. The macromolecular properties of the solutions and hydrogels at a concentration of 0.5 mg mL^{-1} were analyzed by SEC with MALLS detection, in terms of the SEC weight distributions, $w(\log V_h)$, and the size dependence of the weight-average molecular weight distribution, $\bar{M}_w(V_h)$ (Fig. 3a). Using DMSO-LiBr as the solvent and mobile phase of the SEC-MALLS, the molecular dissolution of the macromolecules was promoted, without disrupting the covalent crosslinks and preventing aggregative effects common in aqueous solvents. CAX exhibited a monomodal size distribution centered at a hydrodynamic radius, R_h

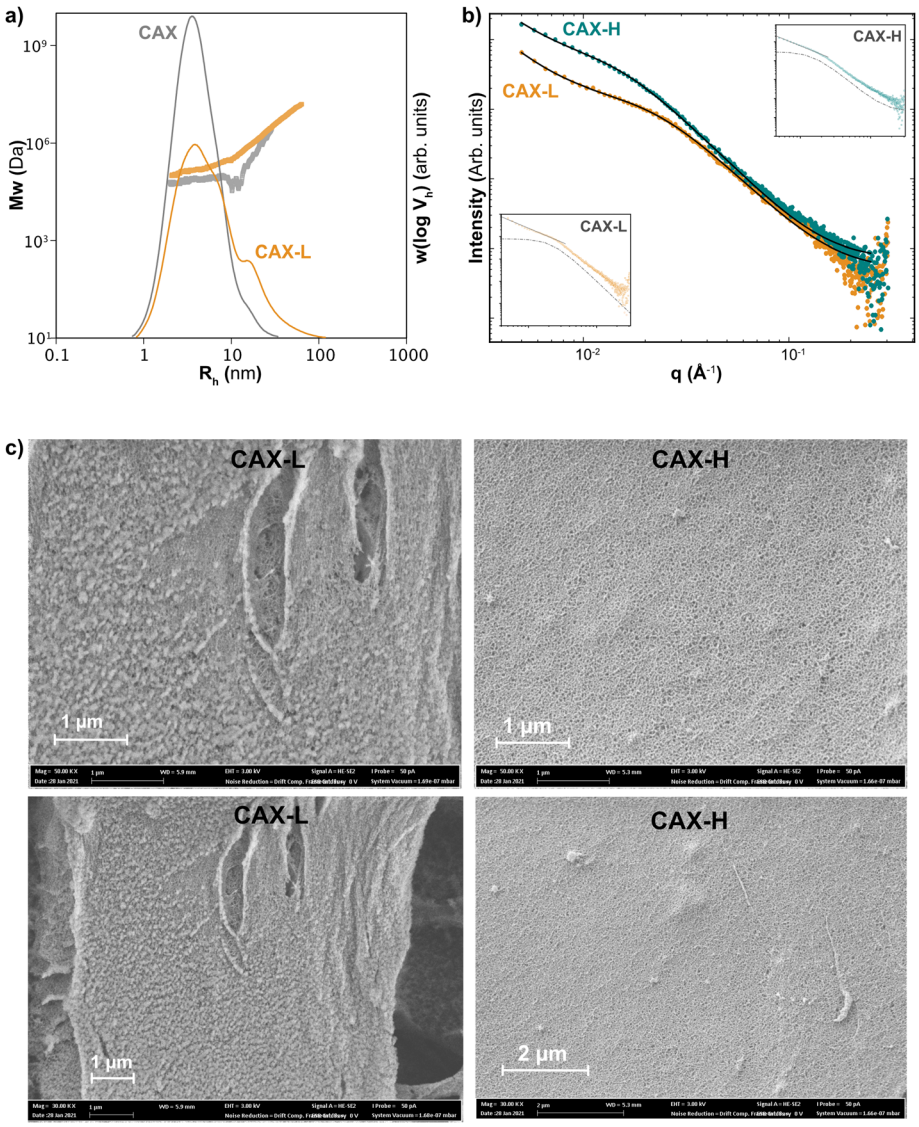

Fig. 3 Size and structure of native (CAX), laccase-crosslinked (CAX-L) and HRP-crosslinked (CAX-H) AX (a) molar mass distributions of CAX and CAX-L; (b) experimental SAXS data and fittings with eqn (1) for CAX-L and CAX-H. An excellent agreement is achieved. Insets: scattering from CAX-L and CAX-H showing the two components of the model; the Lorentzian with dashed line and the power-law with solid line; and (c) scanning electron micrographs showing the microstructure of CAX-L and CAX-H at two magnifications (50 kX: above; 30 kX: below).

of 4.1 nm, corresponding with high molar mass AX populations of 8.3×10^4 Da, in agreement with previous studies.[16] Interestingly, the molar mass distribution of CAX-L displayed a shift of the $w(\log V_h)$ to lower sizes compared to the native CAX and the occurrence of a shoulder at R_h sizes over 10 nm, together with a higher absolute molar mass $[M_w(V_h)]$ at a certain hydrodynamic size (R_h). The increase in $\bar{M}_w(V_h)$ together with the decrease in $w(\log V_h)$ indicates the presence of covalent crosslinks between AX chains and more compact hydrodynamic conformations of CAX-L induced by the laccase treatment. Higher concentrations of CAX and CAX-L (1.0 and 2.0 mg mL^{-1}) were also tested in SEC-MALLS for comparison (ESI, Fig. S5†). This further confirmed the occurrence of more compact hydrodynamic conformations following the enzymatic crosslinking (CAX-L). As for CAX-H, the size distribution could not be accurately detected by SEC-MALLS, as we believe it was filtered out in the sample preparation step prior to injection. This may indicate the occurrence of larger covalent crosslinked polymeric architectures in CAX-H that are filtered out prior to SEC injection and hence prevent their analysis. This might be partly explained by the different specificity of laccase and HRP towards polyphenols, as laccase seems to act preferentially on smaller polyphenols in early lignification stages and HRP can act on larger polymeric moieties and lignin-carbohydrate complexes,[39,40] thus inducing the covalent crosslinking of larger polymeric assemblies compared to laccase. However, this hypothesis would still require experimental demonstration.

The network structure of CAX-L and CAX-H at the nanoscale level was investigated by WAXS and SAXS. WAXS revealed that the structure of the corn hydrogels is amorphous at the macromolecular level (ESI, Fig. S6†), which is related to the largely substituted nature of corn AX that prevents backbone interactions. This is different to our gels prepared using feruloylated AX from wheat bran (W-AX) with low degree of substitution, which show clear crystalline structures in WAXS due to the possibility of backbone interactions, as previously reported.[26]

The SAXS intensity, $I(q)$, was fitted with the correlation length model described in eqn (1):

$$I(q) = \frac{A}{q^n} + \frac{C}{1 + (q\xi)^m} + B \quad (1)$$

Here, n is the power-law exponent, A is the power-law coefficient, m is the Lorentz exponent, C is the Lorentz coefficient, ξ is the correlation length for the polymer chains and B is the background. This model is suitable for the study of the network structure of polymeric assemblies in gel systems and proposes correlations in two different length scales (*i.e.* for the crosslinked AX polymers and the aggregates, respectively), without considering the influence of the pores on the scattering pattern. The first term describes the power-law scattering from larger clusters in the low q region (exponent n). The second term, the Lorentzian, describes the scattering from polymer chains in high q (exponent m).[41] The correlation length, ξ is the indication of the size of growing aggregates in chemical gels.[42,43] The fitting of the data is shown in Fig. 3b and the fitting parameters are presented in Table 2.

In the high q range, the high Lorentz exponents of both hydrogels (m = 3) showed the presence of compact polymer coils (polymer globules).[44] The Lorentz exponents (m) of both hydrogels were similar, indicating similar compactness of the individual polymer chains in these hydrogels. Interestingly, the correlation length (ξ), which is used to characterize the local chain networks in the hydrogels, was higher for CAX-H than that for CAX-L. Therefore, CAX-H seems to form larger polymeric assemblies compared to CAX-L, in agreement with the previous discussion from the SEC-MALLS results.

In the low q regime, CAX-L and CAX-H may be described as mass fractals as the power-law exponent, n of both hydrogels was in the range of $1 < n < 3$. However, comparing both samples, CAX-L has a marked higher value of the power-law coefficient A compared to CAX-H, which indicates that the term in eqn (1) related to larger clusters has a more significant contribution in the laccase crosslinked hydrogels compared to the peroxidase ones. These results suggest that cluster formation seems to be promoted by laccase compared to peroxidase, resulting in a larger contribution to the overall gel multiscale structure and performance. This difference may account for the higher network strength of CAX-L observed by the rheological measurements.

The smaller correlation length (ξ) but higher clustering ability of CAX-L suggests that the slow crosslinking by laccase induces smaller polymeric aggregates that likely facilitate their nucleation into more organized and homogeneous network clusters, which result in more elastic hydrogels. On the other hand, the quick crosslinking reaction by HRP forms larger (higher ξ) but potentially more heterogeneous polymeric aggregates in CAX-H, which may hinder their subsequent cluster formation and hence, result in lower clustering strength. Overall, the SAXS results reveal the structural differences between the CAX-L and CAX-H hydrogels at the nanometric level, which influence their size distributions and the rheological properties.

The microstructure of CAX-L and CAX-H analyzed by SEM is shown in Fig. 3c and the total porosity values of the two hydrogels are presented in Table 2. Both hydrogels showed a porous structure, with CAX-L having less porosity than CAX-H. The lower porosity of the CAX-L hydrogel, together with the formation of network clusters as revealed by SAXS measurements, again reinforces the hypothesis of a more organized network assembly of the corn AX chains during the slower crosslinking reaction by laccase, which results in higher elastic properties and a lower viscous contribution compared to CAX-H.

Table 2 Fitting parameters of the correlation length model of SAXS data and porosity from SEM analysis for of CAX hydrogels

	n	m	ξ (Å)	A	C	Porosity (%)
CAX-L	2.6 ± 0.6	2.9 ± 1.7	44 ± 15	2.6×10^{-5}	9.8 ± 2.9	26.88
CAX-H	2.7 ± 0.3	3.0 ± 0.6	67 ± 8	1.3×10^{-5}	9.8 ± 1.2	36.76

Corn AX hydrogels are biocompatible and provide protection against oxidative stress

Biocompatible polysaccharide-based hydrogels have been widely used for wound healing and tissue engineering.[45,46] As the FA motifs present in AX have antioxidant properties,[16,47–49] we wanted to test the radical scavenging potential of corn bran AX hydrogels targeting reactive oxygen species produced by human colon cells. We seeded human epithelial cell line (HT-29-MTX) on top of the CAX-L and CAX-H hydrogels and studied their cyto-compatibility and antioxidant activity against TBHP-induced oxidative stress compared to an alginate gel. Polymeric alginate was selected as reference material as it has been shown not to convey any antioxidant activity unless depolymerized to its smaller fractions by enzymatic hydrolysis or radiation.[50–52] The ROS production of the cells on alginate gradually increased over time and with increasing TBHP concentration (Fig. 4a). This indicated that HT-29-MTX cells are likely to suffer injury on alginate when exposed to oxidative stress, as supported by the lower cell viability with increasing TBHP concentration (Fig. 4d). On the contrary, the cells cultured on CAX-L and CAX-H produced lower ROS at each time point for all the TBHP concentrations applied (Fig. 4b and c). This implied that both CAX-L and CAX-H were able to suppress the ROS produced by the cells. This action of CAX-L and CAX-H can be attributed to the feruloylation of the CAX substrate, which is known to carry antioxidant activity against

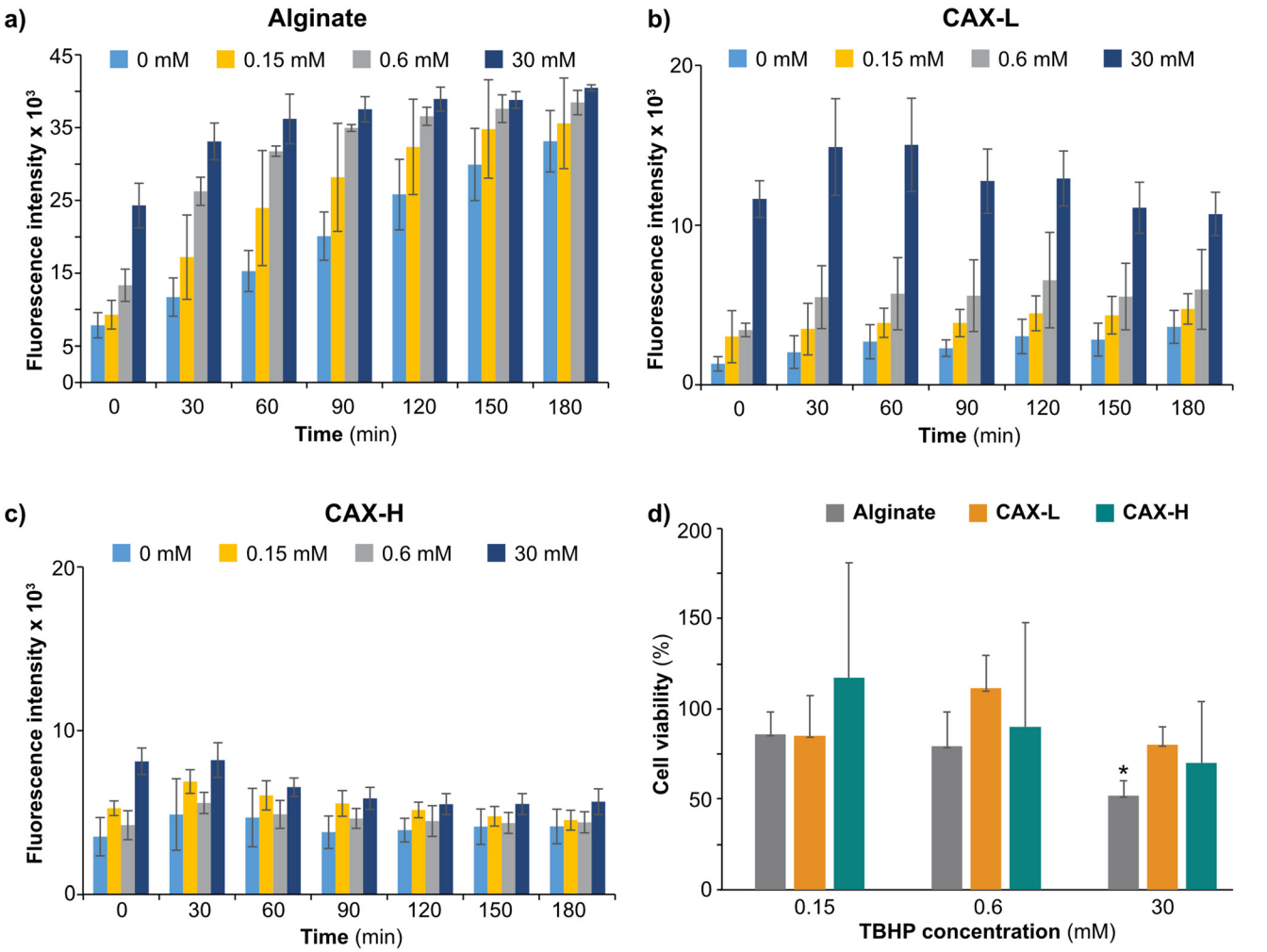

Fig. 4 Cellular ROS production after exposure to different concentrations of TBHP (0, 0.15, 0.6 and 30 mM)-induced oxidative stress of (a) alginate gel, (b) CAX-L hydrogel, (c) CAX-H hydrogel and (d) viability of HT-29-MTX cells after 3 h exposure to TBHP-induced oxidative stress. Statistical differences were calculated by one-way ANOVA using Prism (9.0) and * indicate p values of <0.05.

both intracellular and extracellular ROS.[53] The cell viability measured in the presence of TBHP further confirmed the antioxidant function of the CAX hydrogels (Fig. 4d). For both CAX-L and CAX-H, the cell viability was still over 70% (85% for CAX-L and 70 for CAX-H) with TBHP concentrations from 0.15 mM to 30 mM. The high deviation of the cell viability values for the CAX-H hydrogels was due to the heterogeneous surface of the hydrogel, which resulted in large background differences in the measurements. Interestingly, the viability of the cells in the alginate gel significantly decreased with the increased TBHP concentration, and a cell viability of 52% was measured on alginate containing 30 mM TBHP.

As for CAX-L alone (Fig. 4b), the ROS production gradually increased when the TBHP concentration increased and more importantly, it remained almost constant over the course of the measurement for the concentrations of 0, 0.15 and 0.6 mM. When the TBHP concentration was increased to 30 mM, cells produced substantially higher ROS due to excessive oxidative stress. This was also correlated with the lower viability of the cells at this concentration (Fig. 4d), suggesting that the cells neither survived such high oxidative stress nor CAX-L was able to protect cells from such high ROS amounts. CAX-H, on the other hand, yielded rather constant values in terms of ROS production with increasing TBHP concentrations. Furthermore, the ROS production at the highest TBHP concentration (30 mM) was lower than that observed for CAX-L, suggesting a higher antioxidant activity of CAX-H than CAX-L. This may be attributed to the higher porosity of CAX-H, which provides a larger surface area to scavenge ROS.

Overall, the hydrogels produced by the crosslinking of corn bran F-AX protected HT-29-MTX cells against oxidative stress induced by lower concentrations of TBHP. This protection was higher in the case of CAX-H, while CAX-L provided a more elastic gel network. Therefore, we speculate that CAX-H would provide better resistance to cells against oxidative stress by triggering their antioxidant defense systems, whereas CAX-L might provide a better load-bearing scaffold for biomedical applications due to its higher network elasticity. To the best of

our knowledge, F-AX hydrogels have not been tested for their potential against oxidation in direct contact with cells. Thus, we anticipate that the results of the present study would have important implications for future biomedical and nutritional applications of feruloylated AX hydrogels.

Biomedical applications of polysaccharide-based hydrogels are limited due to their weak mechanical properties, which are usually enhanced by blending with other polymers[54] or by processing techniques[55] to provide durable scaffolds. Our enzymatically produced hydrogels exhibit comparable rheological properties to those produced as such polysaccharide composites/processed materials,[54,56] without a need for additional treatments. It is well known that oxidative stress hinders the healing of chronic wounds.[46] Our polysaccharide hydrogels could be then used as matrices for wound healing since they would prevent oxidative stress and facilitate the healing process as well as providing mechanically strong matrices. On the other hand, cereal AX are well known dietary fibres that are remain undigested in the upper gastrointestinal tract, but can be fermented by beneficial bacteria when they reach the colon exhibiting prebiotic properties.[57,58] Our corn AX hydrogels could be then used in nutritional applications for controlled delivery of active compounds (*e.g.* probiotics and drugs) to the gut, combining the prebiotic properties derived from their fermentation by beneficial gut bacteria and their radical scavenging activity protecting epithelial gut layers against oxidative processes, thus modulating gut microbiota and improving gut health.

Conclusions

We have demonstrated *in vitro* the protective effect against cellular oxidative stress of hydrogels prepared from corn bran feruloylated arabinoxylans using laccase/O_2 and peroxidase/H_2O_2 crosslinking. The proposed chemo-enzymatic process to generate the hydrogels from corn fibre offers multiple environmental and functional advantages over other routes. On one side, it utilizes a widely available side stream from the primary sector (corn fibre). On the other hand, the extraction process by subcritical water is energy efficient, industrially scalable, and environmentally benign, as it only uses water as solvent without additional chemicals or catalysts. Finally, the oxidative biocatalytical route by laccase/peroxidase is extremely mild (operates at room temperature and water) and only requires minimal addition of cosubstrate (O_2 and H_2O_2). Peroxidase induced gelation occurred strikingly faster than that by laccase and the conversion of monomeric ferulic acid to its dehydrodimers and dehydrotrimers was slightly higher. Rheological analysis showed that the hydrogel network formed by laccase crosslinking was more elastic than that obtained by peroxidase. Size chromatography, small angle X-ray scattering, and microstructure analyses suggested the formation of larger covalent crosslinked polymer aggregates and a more heterogeneous cluster network when peroxidase was used as the crosslinking enzyme. Conversely, the laccase-formed hydrogel was composed of smaller polymeric aggregates with higher clustering ability, potentially induced by the slower crosslinking kinetics of this enzyme system. The applicability of the two hydrogels was tested in terms of the protection against oxidative stress on human colon cells as compared to alginate gel as a reference. Both laccase- and peroxidase-crosslinked hydrogels exhibited scavenging activity of chemically induced oxidative stress, indicating their protective potential in cell applications under oxidative stress. In terms of the antioxidative potential, the peroxidase-crosslinked hydrogel showed higher protection against oxidants. Therefore, both laccase- and peroxidase-crosslinked AX hydrogels show large potential for biomedical and nutraceutical applications due to their combined mechanical strength, antioxidant potential and biocompatibility, which could be exploited for wound healing, cellular damage repair, and targeted delivery of functional compounds (*i.e.* probiotic bacteria and biological drugs) to the gut.

Conflicts of interest

There are no conflicts to declare.

Acknowledgements

The authors acknowledge the financial support to the project BARBARA (Biopolymers with advanced functionalities for building and automotive parts processed through additive manufacturing) from the Bio Based Industries Joint Undertaking under the European Union's Horizon 2020 research and innovation programme (grant agreement no. 745578), the Swedish Research Council Formas (Project 942-2016-119) and the Lantmännen Research Foundation (Project 2016F008). Access to SAXS and cryo-SEM infrastructure was supported by Vinnova's grant for Use and Competence Building – MAX IV and ESS (Project 2020-00836) and Treesearch – The Swedish National Infrastructure for New Materials from Trees. We acknowledge MAX IV Laboratory for time on Beamline CoSAXS under Proposal 20200706, which confirmed the SAXS data hereby presented. Research conducted at MAX IV, a Swedish national user facility, is supported by the Swedish Research council under contract 2018-07152, the Swedish Governmental Agency for Innovation Systems under contract 2018-04969, and Formas under contract 2019-02496. Stéphane Kohnen and Mahmoud Hamzoui from Celabor Biomass Valorization (Extraction) are acknowledged for providing the corn bran extracts. The authors acknowledge the access to the facilities and the technical assistance of the Umeå Centre for Electron Microscopy – National Microscopy Infrastructure (UCEM-NMI) and Chalmers University Materials Analysis Laboratory. Dr Cheng Choo Lee, Dr Sara Henriksson and Dr Barbara Berke are acknowledged for their technical and scientific assistance. This work benefited from the use of the SasView application, originally developed under NSF award DMR-0520547. SasView

contains code developed with funding from the European Union's Horizon 2020 research and innovation program under the SINE2020 project, grant agreement No 654000.

References

1 U. N. E. Programme, *Food Waste Index Report 2021*, United Nations Environment Programme, Nairobi, 2021.
2 F. United Nations Food and Agriculture Organization, *Technical Platform on the Measurement and Reduction of Food Loss and Waste*, (accessed 16/07/2022).
3 C. G. Otoni, H. M. C. Azeredo, B. D. Mattos, M. Beaumont, D. S. Correa and O. J. Rojas, The Food–Materials Nexus: Next Generation Bioplastics and Advanced Materials from Agri-Food Residues, *Adv. Mater.*, 2021, **33**(43), 2102520, DOI: **10.1002/adma.202102520**.
4 F. United Nations Food and Agriculture Organization, *FAOSTAT Crops and livestock products*, **https://www.fao.org/faostat/en/#data/QCL/visualize**, (accessed 16/07/2022).
5 M. S. Izydorczyk and C. G. Biliaderis, Cereal arabinoxylans: advances in structure and physicochemical properties, *Carbohydr. Polym.*, 1995, **28**(1), 33–48, DOI: **10.1016/0144-8617(95)00077-1**.
6 Y. Cao and R. Mezzenga, Design principles of food gels, *Nat. Food*, 2020, **1**(2), 106–118, DOI: **10.1038/s43016-019-0009-x**.
7 N. Reddy, R. Reddy and Q. Jiang, Crosslinking biopolymers for biomedical applications, *Trends Biotechnol.*, 2015, **33**(6), 362–369, DOI: **10.1016/j.tibtech.2015.03.008**.
8 C. Dispenza, S. Todaro, D. Bulone, M. A. Sabatino, G. Ghersi, P. L. San Biagio and C. Lo Presti, Physico-chemical and mechanical characterization of in-situ forming xyloglucan gels incorporating a growth factor to promote cartilage reconstruction, *Mater. Sci. Eng., C*, 2017, **70**(Pt 1), 745–752, DOI: **10.1016/j.msec.2016.09.045**.
9 W. Q. Kong, C. D. Gao, S. F. Hu, J. L. Ren, L. H. Zhao and R. C. Sun, Xylan-Modified-Based Hydrogels with Temperature/pH Dual Sensitivity and Controllable Drug Delivery Behavior, *Materials*, 2017, **10**(3), 304, DOI: **10.3390/ma10030304**.
10 K. Markstedt, W. Xu, J. Liu, C. Xu and P. Gatenholm, Synthesis of tunable hydrogels based on O-acetyl-galactoglucomannans from spruce, *Carbohydr. Polym.*, 2017, **157**, 1349–1357, DOI: **10.1016/j.carbpol.2016.11.009**.
11 T. Kim and T. Hyeon, Applications of inorganic nanoparticles as therapeutic agents, *Nanotechnology*, 2013, **25**(1), 012001.
12 R. Casadey, M. Broglia, C. Barbero, S. Criado and C. Rivarola, Controlled release systems of natural phenolic antioxidants encapsulated inside biocompatible hydrogels, *React. Funct. Polym.*, 2020, **156**, 104729, DOI: **10.1016/j.reactfunctpolym.2020.104729**.
13 M. Hussain, H. Suo, Y. Xie, K. Wang, H. Wang, Z. Hou, Y. Gao, L. Zhang, J. Tao, H. Jiang and J. Zhu, Dopamine-Substituted Multidomain Peptide Hydrogel with Inherent Antimicrobial Activity and Antioxidant Capability for Infected Wound Healing, *ACS Appl. Mater. Interfaces*, 2021, **13**(25), 29380–29391, DOI: **10.1021/acsami.1c07656**.
14 L. Saulnier, J. Vigouroux and J. F. Thibault, Isolation and partial characterization of feruloylated oligosaccharides from maize bran, *Carbohydr. Res.*, 1995, **272**(2), 241–253, DOI: **10.1016/0008-6215(95)00053-v**.
15 L. Saulnier and J. F. Thibault, Ferulic acid and diferulic acids as components of sugar-beet pectins and maize bran heteroxylans, *J. Sci. Food Agric.*, 1999, **79**(3), 396–402, DOI: **10.1002/(SICI)1097-0010(19990301)79:3<396::AID-JSFA262>3.0.CO;2-B**.
16 R. C. Rudjito, A. Jiménez-Quero, M. Hamzaoui, S. Kohnen and F. Vilaplana, Tuning the molar mass and substitution pattern of complex xylans from corn fibre using subcritical water extraction, *Green Chem.*, 2020, **22**, 8337–8352, DOI: **10.1039/D0GC02897E**.
17 A. C. Ruthes, A. Martínez-Abad, H.-T. Tan, V. Bulone and F. Vilaplana, Sequential fractionation of feruloylated hemicelluloses and oligosaccharides from wheat bran using subcritical water and xylanolytic enzymes, *Green Chem.*, 2017, **19**(8), 1919–1931, DOI: **10.1039/c6gc03473j**.
18 S. Yilmaz-Turan, A. Jiménez-Quero, R. Moriana, E. Arte, K. Katina and F. Vilaplana, Cascade extraction of proteins and feruloylated arabinoxylans from wheat bran, *Food Chem.*, 2020, **333**, 127491, DOI: **10.1016/j.foodchem.2020.127491**.
19 E. Carvajal-Millan, B. Guigliarelli, V. Belle, X. Rouau and V. Micard, Storage stability of laccase induced arabinoxylan gels, *Carbohydr. Polym.*, 2005, **59**(2), 181–188, DOI: **10.1016/j.carbpol.2004.09.008**.
20 L. Munk, J. Muschiol, K. Li, M. Liu, A. Perzon, S. Meier, P. Ulvskov and A. S. Meyer, Selective Enzymatic Release and Gel Formation by Cross-Linking of Feruloylated Glucurono-Arabinoxylan from Corn Bran, *ACS Sustainable Chem. Eng.*, 2020, **8**(22), 8164–8174, DOI: **10.1021/acssuschemeng.0c00663**.
21 X. Li, S. Li, X. Liang, D. J. McClements, X. Liu and F. Liu, Applications of oxidases in modification of food molecules and colloidal systems: Laccase, peroxidase and tyrosinase, *Trends Food Sci. Technol.*, 2020, **103**, 78–93, DOI: **10.1016/j.tifs.2020.06.014**.
22 M. C. Figueroa-Espinoza and X. Rouau, Oxidative Cross-Linking of Pentosans by a Fungal Laccase and Horseradish Peroxidase: Mechanism of Linkage Between Feruloylated Arabinoxylans, *Cereal Chem.*, 1998, **75**(2), 259–265, DOI: **10.1094/cchem.1998.75.2.259**.
23 A. L. Martinez-Lopez, E. Carvajal-Millan, J. Marquez-Escalante, A. C. Campa-Mada, A. Rascon-Chu, Y. L. Lopez-Franco and J. Lizardi-Mendoza, Enzymatic cross-linking of ferulated arabinoxylan: effect of laccase or peroxidase catalysis on the gel characteristics, *Food Sci. Biotechnol.*, 2019, **28**(2), 311–318, DOI: **10.1007/s10068-018-0488-9**.
24 D. N. A. Zaidel, I. S. Chronakis and A. S. Meyer, Enzyme catalyzed oxidative gelation of sugar beet pectin: Kinetics and rheology, *Food Hydrocolloids*, 2012, **28**(1), 130–140, DOI: **10.1016/j.foodhyd.2011.12.015**.

25 R. C. Rudjito, A. Jiménez-Quero, M. Hamzaoui, S. Kohnen and F. Vilaplana, Tuning the molar mass and substitution pattern of complex xylans from corn fibre using subcritical water extraction, *Green Chem.*, 2020, **22**(23), 8337–8352, DOI: 10.1039/D0GC02897E.

26 S. Yilmaz-Turan, P. Lopez-Sanchez, A. Jiménez-Quero, T. S. Plivelic and F. Vilaplana, Revealing the mechanisms of hydrogel formation by laccase crosslinking and regeneration of feruloylated arabinoxylan from wheat bran, *Food Hydrocolloids*, 2022, **128**, 107575, DOI: 10.1016/j.foodhyd.2022.107575.

27 C. Menzel, C. Gonzalez-Martinez, A. Chiralt and F. Vilaplana, Antioxidant starch films containing sunflower hull extracts, *Carbohydr. Polym.*, 2019, **214**, 142–151, DOI: 10.1016/j.carbpol.2019.03.022.

28 F. Vilaplana and R. G. Gilbert, Characterization of branched polysaccharides using multiple-detection size separation techniques, *J. Sep. Sci.*, 2010, **33**(22), 3537–3554, DOI: 10.1002/jssc.201000525.

29 K. Manalastas-Cantos, P. V. Konarev, N. R. Hajizadeh, A. G. Kikhney, M. V. Petoukhov, D. S. Molodenskiy, A. Panjkovich, H. D. T. Mertens, A. Gruzinov, C. Borges, C. M. Jeffries, D. I. Svergun and D. Franke, ATSAS 3.0: expanded functionality and new tools for small-angle scattering data analysis, *J. Appl. Crystallogr.*, 2021, **54**(1), 343–355, DOI: 10.1107/S1600576720013412.

30 SasView, https://www.sasview.org/ (accessed Jan 1, 2021).

31 M. Gagnon, A. Zihler Berner, N. Chervet, C. Chassard and C. Lacroix, Comparison of the Caco-2, HT-29 and the mucus-secreting HT29-MTX intestinal cell models to investigate Salmonella adhesion and invasion, *J. Microbiol. Methods*, 2013, **94**(3), 274–279, DOI: 10.1016/j.mimet.2013.06.027.

32 X. Zhang, T. Chen, J. Lim, F. Gu, F. Fang, L. Cheng, O. H. Campanella and B. R. Hamaker, Acid gelation of soluble laccase-crosslinked corn bran arabinoxylan and possible gel formation mechanism, *Food Hydrocolloids*, 2019, **92**, 1–9, DOI: 10.1016/j.foodhyd.2019.01.032.

33 L. Wang, L. Zhang, S. Qiu, C. Liu, P. Zhang, L. Yin and F. Chen, Rheological properties and structural characteristics of arabinoxylan hydrogels prepared from three wheat bran sources, *J. Cereal Sci.*, 2019, **88**, 79–86, DOI: 10.1016/j.jcs.2019.05.003.

34 F. E. Ayala-Soto, S. O. Serna-Saldívar, S. García-Lara and E. Pérez-Carrillo, Hydroxycinnamic acids, sugar composition and antioxidant capacity of arabinoxylans extracted from different maize fiber sources, *Food Hydrocolloids*, 2014, **35**, 471–475, DOI: 10.1016/j.foodhyd.2013.07.004.

35 Q. Yan, X. Tang, B. Zhang, C. Wang, S. Deng, X. Ma, C. Wang, D. Li, S. Huang and P. Dong, Biocatalytic oxidation of flavone analogues mediated by general biocatalysts: horseradish peroxidase and laccase, *RSC Adv.*, 2019, **9**(23), 13325–13331, DOI: 10.1039/c9ra00470j.

36 R. Vismeh, F. Lu, S. P. Chundawat, J. F. Humpula, A. Azarpira, V. Balan, B. E. Dale, J. Ralph and A. D. Jones, Profiling of diferulates (plant cell wall cross-linkers) using ultrahigh-performance liquid chromatography-tandem mass spectrometry, *Analyst*, 2013, **138**(21), 6683–6692, DOI: 10.1039/c3an36709f.

37 M. Bunzel, J. Ralph, C. Funk and H. Steinhart, Structural elucidation of new ferulic acid-containing phenolic dimers and trimers isolated from maize bran, *Tetrahedron Lett.*, 2005, **46**(35), 5845–5850, DOI: 10.1016/j.tetlet.2005.06.140.

38 A. L. Martinez-Lopez, E. Carvajal-Millan, V. Micard, A. Rascon-Chu, F. Brown-Bojorquez, N. Sotelo-Cruz, Y. L. Lopez-Franco and J. Lizardi-Mendoza, In vitro degradation of covalently cross-linked arabinoxylan hydrogels by bifidobacteria, *Carbohydr. Polym.*, 2016, **144**, 76–82, DOI: 10.1016/j.carbpol.2016.02.031.

39 G. Wallace and S. C. Fry, Action of diverse peroxidases and laccases on six cell wall-related phenolic compounds, *Phytochemistry*, 1999, **52**(5), 769–773, DOI: 10.1016/s0031-9422(99)00342-8.

40 P. Oinonen, L. Zhang, M. Lawoko and G. Henriksson, On the formation of lignin polysaccharide networks in Norway spruce, *Phytochemistry*, 2015, **111**, 177–184, DOI: 10.1016/j.phytochem.2014.10.027.

41 B. Hammouda, D. L. Ho and S. Kline, Insight into clustering in poly(ethylene oxide) solutions, *Macromolecules*, 2004, **37**(18), 6932–6937, DOI: 10.1021/ma049623d.

42 F. Bode, M. A. da Silva, P. Smith, C. D. Lorenz, S. McCullen, M. M. Stevens and C. A. Dreiss, Hybrid processes in enzymatically gelled gelatin: impact on, macroscopic properties and cellular response, *Soft Matter*, 2013, **9**(29), 6986–6999, DOI: 10.1039/c3sm00125c.

43 Z. Yang, Y. Hemar, L. Hilliou, E. P. Gilbert, D. J. McGillivray, M. A. Williams and S. Chaieb, Nonlinear behavior of gelatin networks reveals a hierarchical structure, *Biomacromolecules*, 2016, **17**(2), 590–600, DOI: 10.1021/acs.biomac.5b01538.

44 B. Hammouda, *Probing Nanoscale Structures—The SANS Toolbox*, National Institute of Standards Technology Center for Neutron Research, Gaithersburg, MD, 2016, https://www.ncnr.nist.gov/staff/hammouda/the_SANS_toolbox.pdf.

45 H. Hu and F. J. Xu, Rational design and latest advances of polysaccharide-based hydrogels for wound healing, *Biomater. Sci.*, 2020, **8**(8), 2084–2101, DOI: 10.1039/d0bm00055h.

46 T. Zhu, J. Mao, Y. Cheng, H. Liu, L. Lv, M. Ge, S. Li, J. Huang, Z. Chen, H. Li, L. Yang and Y. Lai, Recent Progress of Polysaccharide–Based Hydrogel Interfaces for Wound Healing and Tissue Engineering, *Adv. Mater. Interfaces*, 2019, **6**(17), 1900761, DOI: 10.1002/admi.201900761.

47 Y. H. Cheng, S. H. Yang and F. H. Lin, Thermosensitive chitosan-gelatin-glycerol phosphate hydrogel as a controlled release system of ferulic acid for nucleus pulposus regeneration, *Biomaterials*, 2011, **32**(29), 6953–6961, DOI: 10.1016/j.biomaterials.2011.03.065.

48 D. K. Maurya and T. P. Devasagayam, Antioxidant and prooxidant nature of hydroxycinnamic acid derivatives

ferulic and caffeic acids, *Food Chem. Toxicol.*, 2010, **48**(12), 3369–3373, DOI: **10.1016/j.fct.2010.09.006**.

49 S. Yilmaz-Turan, A. Jiménez-Quero, C. Menzel, D. M. de Carvalho, M. E. Lindström, O. Sevastyanova, R. Moriana and F. Vilaplana, Bio-based films from wheat bran feruloylated arabinoxylan: Effect of extraction technique, acetylation and feruloylation, *Carbohydr. Polym.*, 2020, **250**, 116916, DOI: **10.1016/j.carbpol.2020.116916**.

50 X. Zhao, B. Li, C. Xue and L. Sun, Effect of molecular weight on the antioxidant property of low molecular weight alginate from Laminaria japonica, *J. Appl. Phycol.*, 2011, **24**(2), 295–300, DOI: **10.1007/s10811-011-9679-y**.

51 M. Şen and H. Atik, The antioxidant properties of oligo sodium alginates prepared by radiation-induced degradation in aqueous and hydrogen peroxide solutions, *Radiat. Phys. Chem.*, 2012, **81**(7), 816–822, DOI: **10.1016/j.radphyschem.2012.03.025**.

52 M. Falkeborg, L. Z. Cheong, C. Gianfico, K. M. Sztukiel, K. Kristensen, M. Glasius, X. Xu and Z. Guo, Alginate oligosaccharides: enzymatic preparation and antioxidant property evaluation, *Food Chem.*, 2014, **164**, 185–194, DOI: **10.1016/j.foodchem.2014.05.053**.

53 K. Zdunska, A. Dana, A. Kolodziejczak and H. Rotsztejn, Antioxidant Properties of Ferulic Acid and Its Possible Application, *Skin Pharmacol. Physiol.*, 2018, **31**(6), 332–336, DOI: **10.1159/000491755**.

54 L. Zhang, Y. Ma, X. Pan, S. Chen, H. Zhuang and S. Wang, A composite hydrogel of chitosan/heparin/poly (gamma-glutamic acid) loaded with superoxide dismutase for wound healing, *Carbohydr. Polym.*, 2018, **180**, 168–174, DOI: **10.1016/j.carbpol.2017.10.036**.

55 W. Farhat, R. Venditti, N. Mignard, M. Taha, F. Becquart and A. Ayoub, Polysaccharides and lignin based hydrogels with potential pharmaceutical use as a drug delivery system produced by a reactive extrusion process, *Int. J. Biol. Macromol.*, 2017, **104**(Pt A), 564–575, DOI: **10.1016/j.ijbiomac.2017.06.037**.

56 R. Meena, R. Lehnen and B. Saake, Microwave-assisted synthesis of kC/Xylan/PVP-based blend hydrogel materials: physicochemical and rheological studies, *Cellulose*, 2013, **21**(1), 553–568, DOI: **10.1007/s10570-013-0155-5**.

57 J. Yang, L. B. Bindels, R. R. Segura Munoz, I. Martinez, J. Walter, A. E. Ramer-Tait and D. J. Rose, Disparate Metabolic Responses in Mice Fed a High-Fat Diet Supplemented with Maize-Derived Non-Digestible Feruloylated Oligo- and Polysaccharides Are Linked to Changes in the Gut Microbiota, *PLoS One*, 2016, **11**(1), e0146144, DOI: **10.1371/journal.pone.0146144**.

58 B. R. Hamaker and Y. E. Tuncil, A perspective on the complexity of dietary fiber structures and their potential effect on the gut microbiota, *J. Mol. Biol.*, 2014, **426**(23), 3838–3850, DOI: **10.1016/j.jmb.2014.07.028**.